CHEMISTRY
A EUROPEAN JOURNAL

DOI: 10.1002/chem.200500761

Ruthenium Complexes with the Stanna-*closo*-dodecaborate Ligand: Coexistence of η^1(Sn) and η^3(B–H) Coordination

Torben Gädt,[a] Beatrice Grau,[b] Klaus Eichele,[a] Ingo Pantenburg,[b] and Lars Wesemann*[a]

Abstract: Four stanna-*closo*-dodecaborate complexes of ruthenium have been prepared and characterized by multinuclear NMR studies in solution and in the solid state. The solid-state structures of the dimeric zwitterions $[\{Ru(dppb)(SnB_{11}H_{11})\}_2]$ (**2**) (dppb = bis(diphenylphosphino)butane), $[\{Ru(PPh_3)_2(SnB_{11}H_{11})\}_2]$ (**3**), and the dianionic ruthenium complex $[Bu_3MeN]_2[Ru(dppb)\{2,7,8\text{-}(\mu\text{-}H)_3\text{-}exo\text{-}SnB_{11}H_{11}\}(SnB_{11}H_{11})]$ (**4**) were determined by X-ray crystal structure analysis; they establish an unprecedented structural motif in the chemistry of heteroboranes and transition-metal fragments with the stanna-*closo*-dodecaborate moiety as a two-faced ligand that exhibits η^1(Sn) as well as η^3(B–H) coordination. The η^3-coordinated stannaborate in **4** and in the isostructural compound $[Bu_3MeN]_2[Ru(PPh_3)_2\{2,7,8\text{-}(\mu\text{-}H)_3\text{-}exo\text{-}SnB_{11}H_{11}\}(SnB_{11}H_{11})]$ (**5**) shows fluxional behavior, which was studied in detail by using $^{31}P\{^1H\}$ EXSY and DNMR experiments. The activation parameters for the dynamic process of **5** are given.

Keywords: boron · cluster compounds · NMR spectroscopy · ruthenium · tin

Introduction

A rich structural variety is exhibited by the complexes resulting from the interaction of borane and heteroborane cages with transition-metal fragments; the most common structural motif is the incorporation of the transition metal as a vertex in the borane cage.[1] Stone and co-workers showed that metallaboranes and metallacarboranes are capable of bonding to *exo*-polyhedral transition-metal fragments through direct metal–metal bonds.[2] However, there are relatively few examples of main-group *closo*-heteroboranes bonded to transition-metal moieties through the main-group atom. The longest known representatives of this class are *ortho*-dicarborane–metal complexes with the $[2\text{-Ph-}1,2\text{-}C_2B_{10}H_{10}]^-$ monoanion.[3] More recently, Strauss and co-workers described the first *closo*-monocarborane complex $\{[NBu_4]_2[CuCl(CB_{11}F_{11})]\}$ with an *exo*-polyhedral carbon–metal bond.[4] Another general coordination mode of *closo*-boranes and *closo*-heteroboranes is the formation of up to three agostic B–H–M bonds as established by Lipscomb et al.[5] for $[B_{10}H_{10}]^{2-}$ and by Greenwood et al. for $[B_{12}H_{12}]^{2-}$ in the ruthenium complex $[Ru(PMe_2Ph)_3(B_{12}H_{12})]$.[6] Recent examples of metallacarboranes as tridentate ligands often involve the ruthenium fragment $[RuCl(PPh_3)_2]^+$ and include $[Re(CO)_3(\eta^5\text{-}2,3,10\text{-}(\mu\text{-}H)_3\text{-}exo\text{-}\{RuCl(PPh_3)_2\}\text{-}7,8\text{-}C_2B_9H_8)]$,[7a] $[closo\text{-}2\text{-}(\eta^6\text{-}C_6H_6)\text{-}10,11,12\text{-}\{exo\text{-}RuCl(PPh_3)_2\}\text{-}10,11,12\text{-}(\mu\text{-}H)_3\text{-}2,1\text{-}RuCB_{10}H_7R]$,[7b] $[4\text{-(cod)-}3,7,8\text{-}\{RuCl(PPh_3)_2\}\text{-}3,7,8\text{-}(\mu\text{-}H)_3\text{-}closo\text{-}4,1,6\text{-}RhC_2B_{10}H_9]$,[7c] and $[4\text{-}(\eta^3\text{-}C_3H_5)\text{-}3,7,8\text{-}\{RuCl(PPh_3)_2\}\text{-}3,7,8\text{-}(\mu\text{-}H)_3\text{-}closo\text{-}4,1,6\text{-}NiC_2B_{10}H_9]$.[7d] Furthermore, Teixidor and co-workers described a series of *exo-nido*-ruthenacarboranes featuring conventional S–Ru and P–Ru bonds as well as B–H–Ru agostic bonds.[8a–d]

Several years ago we set out to investigate the coordination abilities of the Group 14 heteroborate $[SnB_{11}H_{11}]^{2-}$ (**1**) towards transition-metal electrophiles.[9] The prevailing coordination mode is the formation of a metal–tin single bond and compounds such as the hexaanionic, square-planar complex $[Pt(SnB_{11}H_{11})_4]^{6-}$ and pentaanionic $[Au(SnB_{11}H_{11})_4]^{5-}$ were obtained as air-stable salts in high yields.[10] In a systematic study of the coordination properties of square-planar platinum complexes we found evidence for the strong *trans*-influence of η^1(Sn)-coordinated stannaborate.[11] More recently, our group showed that $[SnB_{11}H_{11}]^{2-}$ is a ligand of remarkable flexibility when coordinated to gold(I) fragments. In fact, in $[Au_2(PPh_3)_2(SnB_{11}H_{11})_2]^{2-}$ and $[Au_2$-

[a] T. Gädt, K. Eichele, Prof. Dr. L. Wesemann
Institut für Anorganische Chemie der Universität Tübingen
Auf der Morgenstelle 18, Tübingen, 72076 (Germany)
E-mail: lars.wesemann@uni-tuebingen.de

[b] B. Grau, I. Pantenburg
Institut für Anorganische Chemie, Universität zu Köln
Greinstrasse 6, 50939 Köln (Germany)

$(PPh_3)_2(SnB_{11}H_{11})_3]^{4-}$ the stannaborate bridges the Au–Au bond through the tin atom, leading to very short Au–Au distances,[12] whereas it caps an Au_3 triangle in μ_3-mode in $[\{(Et_3P)Au(SnB_{11}H_{11})\}_3]^{3-}$ and an Au_4 rectangle in μ_4-mode in $[\{(dppm)Au_2(SnB_{11}H_{11})_2\}_2]^{4-}$ (dppm = bis(diphenylphosphino)methane).[13]

We report here the preparation and characterization of stannaborate ruthenium complexes with the $[SnB_{11}H_{11}]^{2-}$ moiety coordinated both by three B–H–Ru agostic bonds and a Ru–Sn bond, which establishes an unprecedented structural motif in heteroborane chemistry. Moreover, we give a detailed dynamic NMR analysis of the fluxional behavior of η^3(B–H)-coordinated stannaborate, including the determination of the activation parameters.

Results and Discussion

Synthesis: We chose to react two different, yet closely related ruthenium fragments, $[RuCl_2(dppb)PPh_3]$ and $[RuCl_2(PPh_3)_3]$, with $[SnB_{11}H_{11}]^{2-}$ (**1**) to examine the influence of the chelating phosphane on the formation of structurally different reaction products. We showed in previous work that the reaction of *cis*-$[PtCl_2(PPh_3)_2]$ with two equivalents of **1** yields *trans*-$[Pt(PPh_3)_2(SnB_{11}H_{11})_2]^{2-}$, whereas $[PtCl_2(dppe)]$ leads to *cis*-$[Pt(dppe)(SnB_{11}H_{11})_2]^{2-}$ (dppe = bis(diphenylphosphino)ethane).[14]

Refluxing one equivalent of the sodium salt of stanna-*closo*-dodecaborate with the ruthenium electrophile $[RuCl_2(dppb)PPh_3]$ in THF for 60 h produces the dimeric compound $[\{Ru(dppb)(SnB_{11}H_{11})\}_2]$ (**2**) as an orange precipitate, which can be isolated in rather low yield by filtration and subsequent treatment with water (Scheme 1). Analogously, refluxing $[RuCl_2(PPh_3)_3]$ and $Na_2[SnB_{11}H_{11}]$ in THF for 60 h yields $[\{Ru(PPh_3)_2(SnB_{11}H_{11})\}_2]$ (**3**) as a red precipitate, which can be isolated and purified as described above for **2** (Scheme 2). Both dimeric ruthenium complexes **2** and **3** are stable towards air and moisture. The solubility of **2** is very low, whereas **3** is insoluble in common solvents.

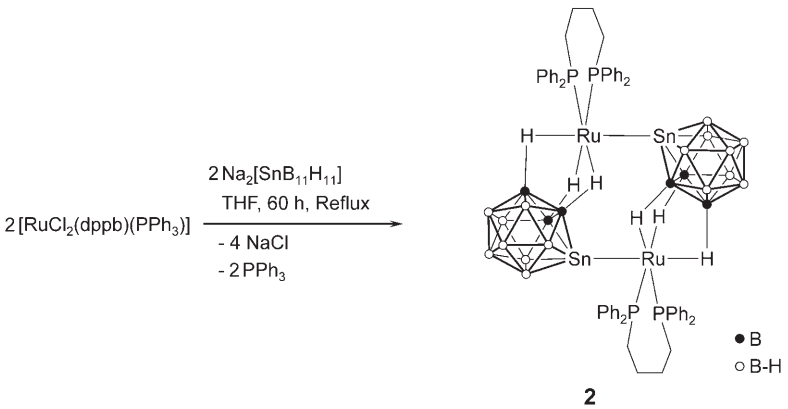

2

Scheme 1. Synthesis of the dimeric ruthenium complex **2**.

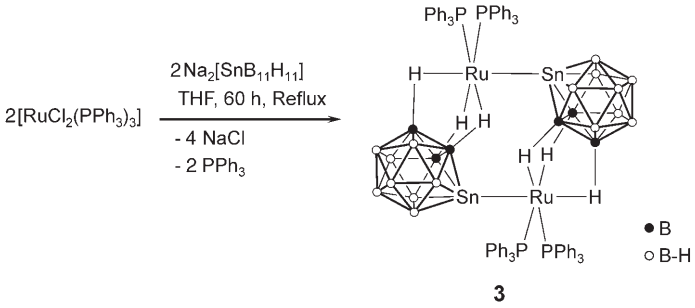

3

Scheme 2. Synthesis of the dimeric ruthenium complex **3**.

To probe whether it would be possible to coordinate two or more stannaborate clusters to a ruthenium fragment, we reacted two equivalents of $[Bu_3MeN]_2[SnB_{11}H_{11}]$ with $[RuCl_2(dppb)(PPh_3)]$ in CH_2Cl_2 at room temperature. The color of the reaction mixture changed from dark green to orange-red. After two hours, the mixture was extracted with water to remove $[Bu_3MeN]Cl$ and CH_2Cl_2 was subsequently evaporated under reduced pressure, yielding $[Bu_3MeN]_2[Ru(dppb)\{2,7,8\text{-}(\mu\text{-}H)_3\text{-}exo\text{-}SnB_{11}H_{11}\}(SnB_{11}H_{11})]$ (**4**) as an orange powder, which was washed several times with Et_2O to remove PPh_3 (Scheme 3). The remaining solid is stable towards air and moisture.

Following a modified protocol described for the synthesis of **4**, we succeeded in isolating $[Bu_3MeN]_2[Ru(PPh_3)_2\{2,7,8\text{-}(\mu\text{-}H)_3\text{-}exo\text{-}SnB_{11}H_{11}\}(SnB_{11}H_{11})]$ (**5**) as a red, air-stable powder starting from $[RuCl_2(PPh_3)_3]$ (Scheme 4).

Solid-state structures: To elucidate the solid-state structures of **2** and **3** we undertook X-ray single-crystal structure analyses. Orange crystals of **2** were obtained by crystallization from CH_2Cl_2. The molecular structure of **2** together with selected interatomic distances and angles is shown in Figure 1 and the crystal data as well as parameters of the structure refinement are given in Table 4.

The heteroborate plays the role of a bridging ligand that uses two different coordination modes, formation of a Ru–Sn bond to one ruthenium atom and formation of three agostic B–H–Ru bonds to the symmetry-equivalent ruthenium atom Ru′. The agostic interactions are inequivalent; the Ru–B(6′) distance (2.353(5) Å) is shorter than the Ru–B(1′) (2.416(4) Å) and Ru–B(2′) distances (2.419(4) Å). Comparable distances have been reported in the literature for similar systems and the inequivalent agostic B–H–Ru interactions have been ascribed to different *trans* influences of the particular *trans*-located li-

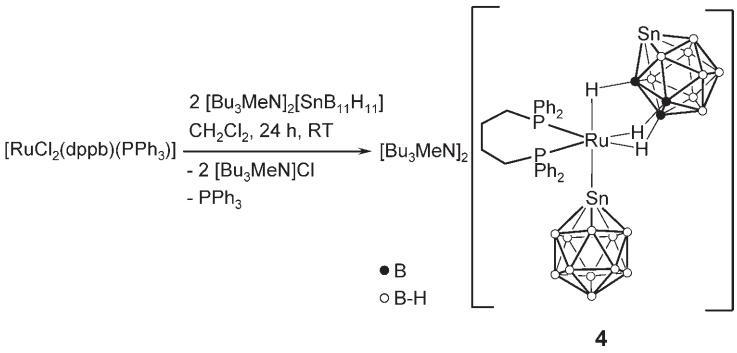

Scheme 3. Synthesis of the dianionic ruthenium complex **4**.

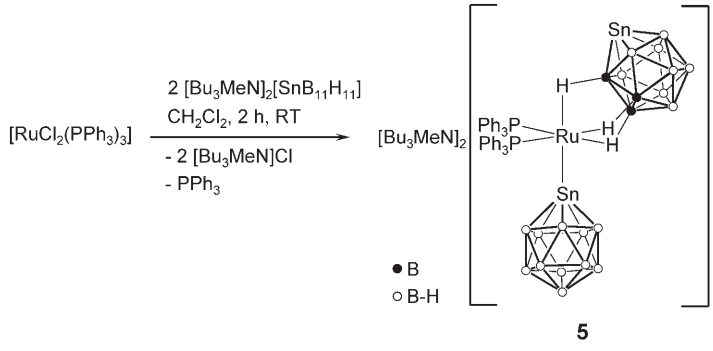

Scheme 4. Synthesis of the dianionic complex **5** with the PPh_3 ligand.

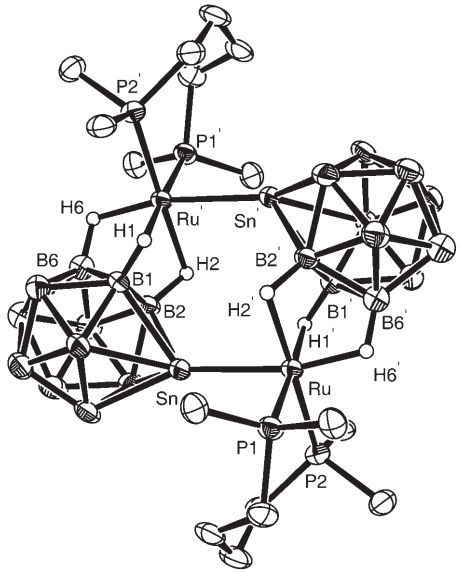

Figure 1. Molecular structure of **2**. The phenyl rings and hydrogen atoms except the *ipso*-carbon and the B–H–Ru hydrogen atoms have been omitted for the sake of clarity. Selected interatomic distances [Å] and angles [°]: Ru–P1 2.293(1), Ru–P2 2.287(1), Ru–Sn 2.576(6), Ru–B1′ 2.416(4), Ru–B2′ 2.419(4), Ru–B6′ 2.353(5), Ru–H1′ 1.93(3), Ru–H2′ 1.90(4), Ru–H6′ 1.70(5); P2-Ru-P1 92.63(4), P1-Ru-Sn 93.94(3), H1′-Ru-P2 86.5(10), H1′-Ru-Sn 82.6(11), H6′-Ru-P2 96.8(16), H6′-Ru-Sn 166.5(17), H6′-Ru-H1′ 89.7(19). Symmetry transformation used to generate equivalent atoms: $1-x, -y+1, -z$.

gand.[8c,15] The Ru–Sn separation (2.576(1) Å) falls in the range of known Ru–Sn lengths (2.55–2.69 Å).[16]

An unusual aspect of the agostic B–H–Ru interaction in the dimeric compound **2** is the fact that the stannaborate **1** uses two B–H vertices from the first B_5-belt and one B–H vertex from the second B_5-belt (Figure 2). As already mentioned in the introduction, the interaction of metallacarboranes with transition-metal fragments through three agostic B–H–M bonds is well established, mainly from the work of Stone and co-workers, but the predominating geometry found is based on the usage of two B–H vertices from the second belt and one B–H vertex from the first belt.[7a,b] The exceptions we could find in the literature are [4-(η^3-C_3H_5)-3,7,8-{$RuCl(PPh_3)_2$}-3,7,8-(μ-H)$_3$-4,1,6-*closo*-$NiC_2B_{10}H_9$], in which the 13-vertex nickeladicarborane is bonded to the ruthenium fragment through two B–H vertices of the first six-membered CBCBBB ring and one B–H vertex of the second B_5-ring,[7d] and the structurally similar rhodadicarborane ruthenium complex [4-(cod)-3,7,8-{$RuCl(PPh_3)_2$}-3,7,8-(μ-H)$_3$-*closo*-4,1,6-$RhC_2B_{10}H_9$].[7c]

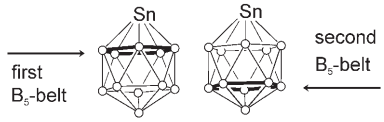

Figure 2. Graphical representation of the B_5-belts of **1**.

A single-crystal X-ray diffraction study of the ruthenium complex **3** revealed that it is in fact a close congener to **2**. An ORTEP plot of the molecular structure is depicted in Figure 3. The distances are very similar to those of the analogous compound **2**, whereas the P2-Ru-P1 angle of 100.01(5)° is slightly larger owing to the steric demand of the triphenylphosphane ligands.

Orange single crystals of dianion **4** were obtained by layering a CH_2Cl_2 solution with hexane. In the molecular structure two stannaborate moieties are coordinated at the ruthenium fragment in different coordination modes. One cluster forms a Ru–Sn bond and the other $[SnB_{11}H_{11}]^{2-}$ moiety has three exopolyhedral agostic B–H–Ru bonds. The tin atom of the η^3-coordinated stannaborate remains uncoordinated by a transition-metal fragment (Figure 4). However, it was soon realized during the structure refinement that some disorder was present in the η^3-coordinated cluster. Repeated crystallizations consistently gave crystals that were disordered in an analogous manner. Indeed, the η^3-coordinated cluster is disordered over two positions with a ratio of 83.3:16.7. The principal orientation **4a** (Figure 4) has **1** coordinated to the ruthenium fragment with one B–H vertex from the first B_5-belt and two B–H vertices from the second B_5-belt. Again the three agostic B–H–Ru bonds are unequal with Ru–B(6) (2.284(4) Å), which lies *trans* to the tin-coordinated stannaborate, being shorter than Ru–B(1) (2.324(2) Å) and Ru–B(7) (2.317(4) Å), in which a phosphane ligand is coordinated in the *trans* position. The ruthe-

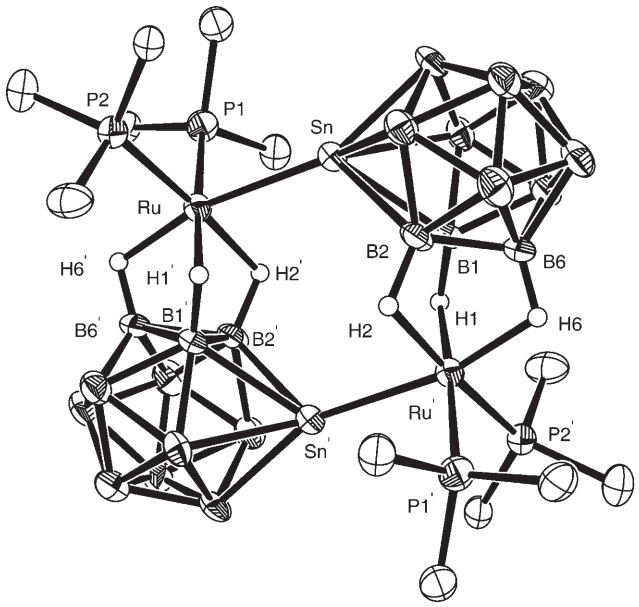

Figure 3. Molecular structure of **3**. The phenyl rings and hydrogen atoms except the *ipso*-carbon and the B–H–Ru hydrogen atoms have been omitted for the sake of clarity. Selected interatomic distances [Å] and angles [°]: P1–Ru 2.326(1), P2–Ru 2.325(1), Ru–H(6′) 1.73(4), Ru–H1′ 1.80(3), Ru–H2′ 1.84(4), Ru–B6′ 2.326(5), Ru–B1′ 2.392(5), Ru–B2′ 2.407(6), Ru–Sn 2.574(1); P2-Ru-P1 100.01(5), P1-Ru-Sn 93.87(4), P2-Ru-Sn 95.84(3), H1′-Ru-P2 80.4(11), H1′-Ru-Sn 83.5(11), H6′-Ru-P2 91.3(13), H6′-Ru-Sn 166.4(13), H6′-Ru-H1′ 86.4(16). Symmetry transformation used to generate equivalent atoms: $-x+1$, $-y+2$, $-z+2$.

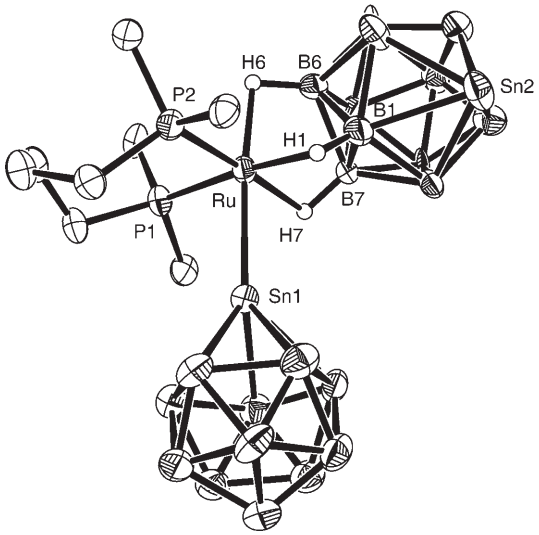

Figure 4. Molecular structure of **4a**. The phenyl rings and hydrogen atoms except the *ipso*-carbon and the B–H–Ru hydrogen atoms have been omitted for the sake of clarity. Selected interatomic distances [Å] and angles [°]: Ru–P1 2.282(2), Ru–P2 2.295(2), Ru–Sn1 2.600(1), Ru–B1 2.324(2), Ru–B6 2.284(4), Ru–B7 2.317(4), Ru–H1 1.83(6), Ru–H6 1.82(6), Ru–H7 1.85(6); P1-Ru-P2 97.17(7), P1-Ru-Sn1 89.99(6), P2-Ru-Sn1 92.80(6), P1-Ru-H7 87.2(19), P1-Ru-H1 174.26(6), P2-Ru-H1 83.87(5), Sn1-Ru-H1 84.31(2), Sn1-Ru-H7 81.3(19).

nium–tin separation Ru–Sn(1) (2.600(1) Å) is slightly larger than for **2** and **3** and the P1-Ru-P2 angle, 97.17(7)°, lies between those already described for **2** and **3**.

The other orientation present, **4b**, has the η^3-coordinated stannaborate cluster employing two B–H vertices from the first B_5-ring and one B–H vertex from the second B_5-ring. This also implies a different orientation of the uncoordinated Sn relative to the other ligands at the ruthenium centre. Both orientations together with other stereoisomers are depicted in Figure 6 (see discussion below). Because **4b** is the minor structural isomer in the solid state, the geometric parameters of **4b** will not be discussed.

NMR spectroscopy in solution: To examine the solution behavior of **2**, a multinuclear NMR study was undertaken. Unfortunately, the solubility of **2** is very limited, which severely hampered the examinations and made the observation of a $^{119}Sn\{^1H\}$ NMR spectrum in solution impossible. The $^{31}P\{^1H\}$ NMR spectrum reveals a sharp singlet at $\delta = 52.2$ ppm with a coupling constant of $^2J(^{117,119}Sn,P) = 288$ Hz ($^{117}Sn/^{119}Sn$ coupling could not be resolved), which unambiguously shows that the solid-state structure remains intact in solution. It is known from the literature that *cis*-$^2J(^{117,119}Sn,P)$ coupling constants range from 270 to 400 Hz for ruthenium complexes.[16] The $^{11}B\{^1H\}$ NMR spectrum shows one relatively sharp signal at $\delta = -31.7$ ppm, whereas the other signals are very broad. Unlike η^1(Sn)-coordinated stannaborate, which typically displays one signal for B2–B6 and B7–B11 because of accidental isochrony, and another for the antipodal B12,[9] the loss of symmetry at the η^3(BH)-coordinated heteroborate moiety causes the occurrence of a higher number of signals in the $^{11}B\{^1H\}$ NMR spectrum. A proton-coupled ^{11}B NMR experiment allowed us to assign the unusually high-field shifted signal at $\delta = -31.7$ ppm to the agostic B–H–Ru boron atoms, since the ^1J(B,H) coupling constant of 92 Hz is characteristically smaller than the coupling constant of free terminal B–H units, which lies between 120 and 190 Hz.[17] The $^1H\{^{11}B\}$ NMR spectrum of **2** exhibited two signals in the high-field region with an integration ratio of 2:1. A doublet at $\delta = -4.85$ ppm with ^2J(P,H) = 30.1 Hz can be assigned to H1 and H2, and a singlet at $\delta = -8.27$ ppm with $^{117,119}Sn$ satellites and $^2J(^{117,119}Sn,H) = 212$ Hz is assigned to H6. A similar $^2J(^{117,119}Sn,H)$ coupling constant has been described for the trinuclear ruthenium cluster $[(\mu\text{-}H)_2(\mu_3\text{-}S)(\mu\text{-}Cl)Ru_3(CO)_8(SnCl_3)]$.[18]

Unfortunately compound **3** is almost completely insoluble in all common solvents, which made solution NMR investigations impossible.

In solution, the $^{31}P\{^1H\}$ NMR spectrum of complex **4** (Figure 5) consists of an A_2 pattern at $\delta = 51.5$ ppm [$^2J(^{117,119}Sn,P) = 267$ Hz] as well as an AB pattern at $\delta = 51.6$ and 51.0 ppm [^2J(P,P) = 35.4 Hz, $^2J(^{117,119}Sn,P) = 273$ Hz]. This strongly indicates that in solution **4** comprises of isomers with different symmetry, that is, C_s and C_1 symmetry (vide infra).

Further evidence comes from a $^{119}Sn\{^1H\}$ NMR measurement of **4**, which shows broad peaks at $\delta = -366$, -374, -630, and -638 ppm with approximately equal intensities. The two peaks around $\delta = -370$ ppm can be assigned to

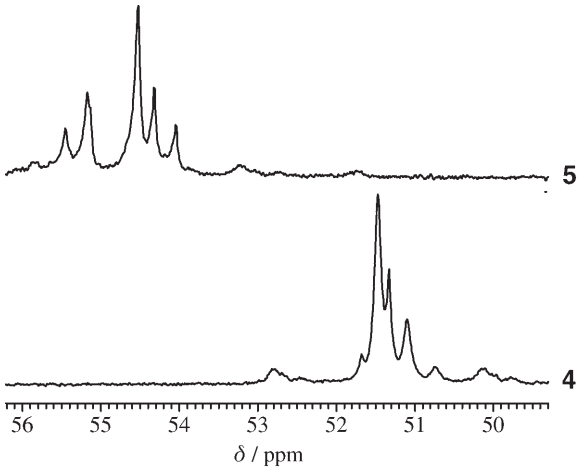

Figure 5. $^{31}P\{^1H\}$ NMR spectra of **4** and **5**, each consisting of an A_2 pattern and an AB pattern.

η^1(Sn)-coordinated stannaborate[9] and the two high-field shifted signals must therefore be assigned to the η^3-coordinated stannaborate. Remarkably, the resonances for the η^3-coordinated heteroborate are high-field shifted relative to free cluster **1**, which shows a broad resonance at $\delta = -546$ ppm.[19] The observation of four signals must be ascribed to the existence of isomeric compounds in solution. The $^{11}B\{^1H\}$ NMR spectrum contains an intense peak at $\delta = -15.2$ ppm, as expected for a η^1(Sn)-coordinated $[SnB_{11}H_{11}]^{2-}$ moiety, which can be assigned to isochronous B2–B6 and B7–B11 in both B_5-rings.[11] Additional broader signals with lower intensity at $\delta = -1.6$, -8.0, and -19.9 ppm, and a relatively sharp signal at $\delta = -22.4$ ppm are ascribed to the η^3-coordinated stannaborate, which has lower local symmetry and thus more resonances than the η^1(Sn)-coordinated cluster. Signals due to B–H–Ru groups could be identified by means of a heteronuclear correlation $^{11}B/^1H$ 2D NMR experiment, which revealed a correlation between the sharp signal at $\delta = -22.4$ ppm in the $^{11}B\{^1H\}$ NMR spectrum and two broad peaks at $\delta = -6.3$ and -7.5 ppm in the ^1H NMR spectrum, which clearly belong to B–H–Ru protons. To overcome the problem of the large linewidth of the hydridic signals, we conducted a $^1H\{^{11}B\}$ NMR experiment that revealed a doublet at $\delta = -7.5$ ppm with a ^2J(H,P) coupling constant of 44.8 Hz and ^{117,119}Sn satellites [$^2J(^{117,119}Sn,H) = 205$ Hz], and a broad multiplet at $\delta = -6.3$ ppm, which lacked a clear coupling pattern. It is known from the literature that coupling constants of the magnitude of the resolved ^2J(P,H) coupling constant are common for *trans*-^2J(P,H) couplings in comparable ruthenium borate complexes.[8c] We therefore conclude that the doublet must be assigned to B–H units in *trans* positions to the phosphane ligand, which implies that ^2J(Sn,H) = 205 Hz is a *cis* coupling (*cis*-^2J(P,H) coupling is not resolved owing to large line widths). Remarkably, the ^{117,119}Sn,H *cis* coupling in **4** is of a magnitude comparable with the *trans* coupling in **2**. A possible explanation could be the anionic character of the complex. In fact, Carlton demonstrated for rhodium-hydrogen-tin systems that $J(^{117,119}Sn,H)$ correlates with the electron density at the rhodium centre and shows a larger response than other coupling constants.[20]

The NMR spectroscopic data for compound **5** are similar to those for **4** (Tables 1 and 2). We thus conclude that **5** is isostructural to **4**. The main differences in the NMR data can be found in the $^{119}Sn\{^1H\}$ NMR and in the $^1H\{^{11}B\}$ NMR spectra. The $^{119}Sn\{^1H\}$ NMR spectrum contains three instead of four signals, but the very broad signal at $\delta = -398$ ppm probably consists of two unresolved peaks. Examination of the ^1H NMR spectrum reveals only a very broad signal at $\delta = -7.3$ ppm, which gains somewhat more structure in the ^{11}B decoupled $^1H\{^{11}B\}$ NMR experiment while retaining an unresolved form; it thus cannot be interpreted unequivocally. $^1H\{^{11}B\}$ NMR experiments at low temperatures lead to no improvement for any of the complexes **2**, **4**, or **5**.

Table 1. Selected $^1H\{^{11}B\}$ NMR and ^{11}B NMR data, δ in ppm, J in Hz.

	$^1H\{^{11}B\}$ Hydride region	^{11}B
2	−4.85 (d, ^2J(P,H) = 30.1), −8.27 (s, $^2J(^{117,119}Sn,H)$ = 212)	−10.8, −15.0, −20.7, −31.7 (^1J(B,H) = 92)
4	−6.2 to −6.5 (br m), −7.5 (d, ^2J(P,H) = 44.8, $^2J(^{117,119}Sn,H)$ = 205)	−1.6, −8.0, −15.2, −19.9, −22.4
5	−7.6 to −7.0 (br)	−2.1, −8.9, −15.3, −20.9

Table 2. $^{31}P\{^1H\}$ NMR and $^{119}Sn\{^1H\}$ NMR data, δ in ppm, J in Hz.

	$^{31}P\{^1H\}$	$^{119}Sn\{^1H\}$
2	52.2 (s, $^2J(^{117,119}Sn,P)$ = 288)	−381[a]
3	53.1, 48.6[a]	−345[a]
4	51.0 (d, ^2J(P,P) = 35.4, $J(^{117,119}Sn,P)$ = 273), 51.5 (s, $^2J(^{117,119}Sn,P)$ = 267), 51.6 (d, ^2J(P,P) = 35.4, $^2J(^{117,119}Sn,P)$ = 273)	−366, −374, −630, −638
5	54.2 (d, ^2J(P,P) = 27.7, $^2J(^{117,119}Sn,H)$ = 260), 54.6 (s, $^2J(^{117,119}Sn,H)$ = 263), 55.4 (d, J(P,P) = 27.7, $^2J(^{117,119}Sn,H)$ = 260)	−398, −628, −640

[a] Solid-state NMR spectroscopy.

Solid-state NMR spectroscopy: Unfortunately, the solubility of compound **2** was not sufficient to allow the detection of $^{119}Sn\{^1H\}$ NMR resonances in solution. We thus conducted a solid-state ^{119}Sn HPDEC/MAS experiment, which displayed a resonance at $\delta = -381$ ppm. This is a chemical shift similar to the solution shifts observed for η^1(Sn)-coordinated **1** in the dianionic ruthenium compounds **4** and **5**. However, the value is somewhat shifted to higher field than hitherto known values, $\delta = -332$ ppm[12] for $[Au_2(PPh_3)_2(SnB_{11}H_{11})_3]^{4-}$ or $\delta = -317$ ppm[10] for $[Pt(SnB_{11}H_{11})_4]^{6-}$, for η^1(Sn) stannaborate on late transition metals. It is shifted down field relative to free $[SnB_{11}H_{11}]^{2-}$ and exclusively η^3-(B–H)-coordinated stannaborate, which appears around $\delta = -630$ ppm (Table 2).

Because compound **3** is insoluble in common solvents we undertook solid-state ^{31}P and ^{119}Sn NMR studies. The ^{31}P VACP/MAS spectrum of **3** showed peaks at $\delta = 53.1$ and 48.7 ppm; these can be assigned to the PPh_3 ligands, which are chemically inequivalent in the solid state. The values are similar to the observed $^{31}P\{^1H\}$ NMR resonances in solution for compounds **2**, **4**, and **5** (Table 2). Owing to the large linewidth in the solid state, no couplings could be resolved. A ^{119}Sn HPDEC/MAS experiment showed a broad signal at $\delta = -345$ ppm, which is shifted somewhat downfield relative to **2**.

Dynamic NMR spectroscopy: Basically, six stereoisomers of **4** and the analogous triphenylphosphane complex **5** can be assumed to exist in solution (Figure 6). Isomer **4a** corresponds to the major isomer present in the solid state and should give rise to an AB pattern in the $^{31}P\{^1H\}$ NMR spectrum; this is also expected for its enantiomer **4a′**. Another isomer **4c** with C_s symmetry can be formulated, which should give an A_2 pattern in the $^{31}P\{^1H\}$ NMR spectrum. Furthermore, corresponding isomers **4b, 4b′,** and **4d**, which exhibit a η^3(B–H) stannaborate coordinated by two B–H vertices from the first B_5-belt and one B–H vertex from the second B_5-belt, have to be considered. An analogous set of isomers **5a–5d** can be devised for the structurally related triphenylphosphane complex **5**. At least two different mechanisms of isomerization can be postulated to cause dynamic interconversion of these isomers. Namely, a rotational twisting **A** of the *exo*-$[Ru(PPh_3)_2(SnB_{11}H_{11})]$ fragment about the cluster face and a translational scrambling **B** of the *exo*-polyhedral ruthenium fragment to the next triangular face of the stannaborate moiety. Stone and co-workers described a similar process for $[2,2,2\text{-}(CO)_3\text{-}2\text{-}PPh_3\text{-}7,8,12\text{-}(\mu\text{-}H)_3\text{-}7,8,12\text{-}\{RuCl(PPh_3)_2\}\text{-}closo\text{-}2,1\text{-}MoCB_{10}H_8]$.[15] Because only one A_2 pattern and one AB pattern are present in the $^{31}P\{^1H\}$ NMR spectra of both **4** and **5**, the simultaneous existence of all six isomers in solution can be ruled out; one would expect two A_2 and two AB systems in the $^{31}P\{^1H\}$ NMR spectra of **4** and **5** if all six isomers were present.

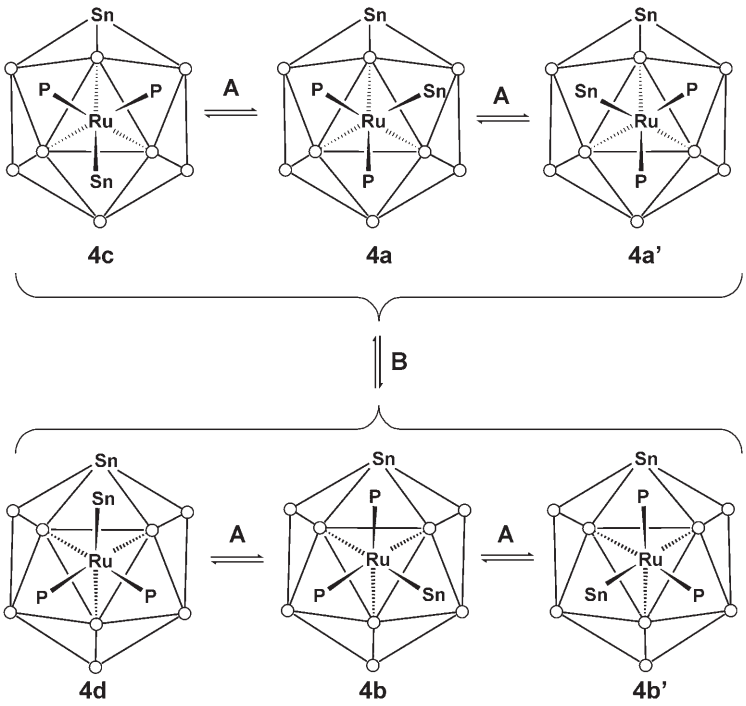

Figure 6. Possible isomeric structures of **4** (and **5**) in solution.

To elucidate the dynamic processes that are responsible for the existence of isomers of both **4** and **5** in solution, we conducted $^{31}P\{^1H\}$ EXSY NMR and selective inversion transfer NMR experiments. Our first objective was to prove unequivocally that both spin systems present interconvert dynamically at room temperature, eliminating the possibility of two independent sets of isomers. We decided to begin with a variable-temperature $^{31}P\{^1H\}$ NMR experiment. At elevated temperatures in a mixture of $MeNO_2$ and $[D_8]$toluene significant line broadening is visible for both **4** and **5**, indicating a dynamic interconversion on the NMR time scale. The spectra for compound **5** (Figure 7) in CD_2Cl_2 display another interesting feature, the temperature dependence of the $^{31}P\{^1H\}$ NMR chemical shifts, which renders the AB system accidentally isochronous at −80 °C and gives rise to two broad singlets with tin satellites. To examine the influence of the solvent we repeated the variable-temperature measurements in $[D_6]$acetone. The temperature dependence of the chemical shift is very similar in acetone. For the AB system the effect is $0.8\,Hz\,K^{-1}$ for both CD_2Cl_2 and acetone in the −80 °C to 20 °C range, while the effect for the A_2 system amounts to $0.6\,Hz\,K^{-1}$ in CD_2Cl_2 and $1.3\,Hz\,K^{-1}$ in acetone. Similar behavior with chemical shift dependencies of up to $3\,Hz\,K^{-1}$ has been reported for the dimeric Pd^I species $[Pd_2(dppm)_2XY]$ (X, Y = Cl, Br, I).[21]

Additionally, a $^{31}P\{^1H\}$ EXSY NMR experiment at room temperature for compound **5** reveals cross-peaks between the A_2 and the AB system, which clearly demonstrates the dynamic character of the interconversion of the spin systems (Figure 8).

To further investigate this dynamic character, we decided to quantitatively determine the activation parameters using selective inversion transfer experiments at different temper-

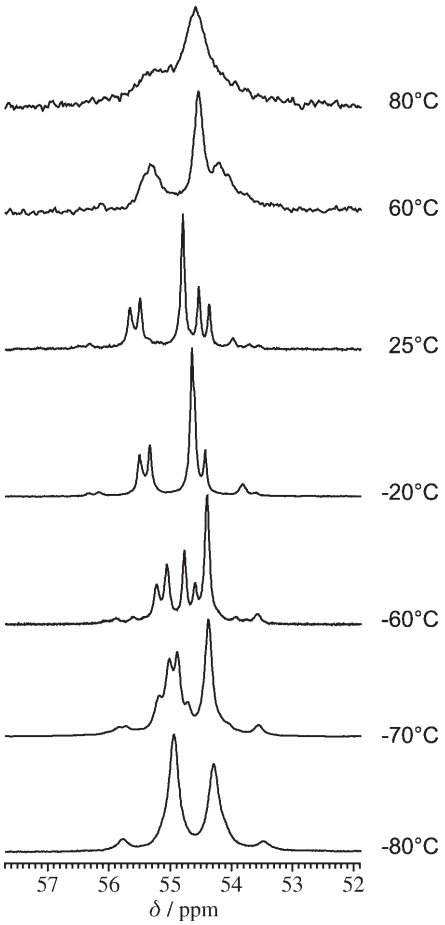

Figure 7. Variable-temperature $^{31}P\{^1H\}$ NMR spectra of **5** in a $MeNO_2$/[D_8]toluene mixture for 60 °C and 80 °C and CD_2Cl_2 for all other temperatures. Note the presence of unresolved $^{117,119}Sn$ satellites for both the AB and A_2 patterns.

atures. Unfortunately, the A_2 and AB spin systems in compound **4** overlap at room temperature (Figure 5), which rendered a quantitative investigation impossible since conventional peak-coalescence methods at higher temperatures are not straightforwardly feasible because of the complexity of the spin systems and the slow exchange process itself. In the analogous complex **5**, on the other hand, the separation is sufficiently large to carry out a quantitative analysis around room temperature.

The regression analysis is shown in Figure 9 and the results are summarized in Table 3. It remains to address the question of which of the two possible processes—rotational twisting of the ruthenium fragment at a triangular face of the stannaborate moiety or translational scrambling of the ruthenium fragment to another triangular face—governs the dynamic interconversion. In a theoretical study, Schleyer and co-workers showed that the translational scrambling process of a dication around the cage faces of *closo*-dodecaborate $[B_{12}H_{12}]^{2-}$ proceeds via a bidentate transition state with the dication coordinating at a cluster edge.[22] The migrational barrier of this face-edge-face process has been reported to be in the range of 8–21 kJ mol^{-1} for monocations and 42–55 kJ mol^{-1} for dications. The value for the dianionic system **5** is 62.7 kJ mol^{-1}, which is a somewhat larger value. If the activation entropy $\Delta S^{\neq} = -27.1$ J mol^{-1} K^{-1} for the interconversion of **5** is taken into account, it seems unlikely that the face-edge-face process, which includes the fission of a B–H–Ru bond, is the rate-determining step. The assumption that rotational twisting of the ruthenium fragment about the triangular face of the stannaborate cluster is responsible for the interconversion of both spin systems seems more plausible given the value of ΔS. We thus conclude that process **A** (Figure 6) dynamically interconverts the isomers **4a**, **4a′**, and **4c** (**5a**, **5a′**, and **5c**) in solution given the fact that **4a** is the major isomer in the solid state.

The rotational twisting is reported to be more rapid for similar systems like [2,2,2-$(CO)_3$-2-PPh_3-7,8,12-(μ-H)$_3$-7,8,12-{$RuCl(PPh_3)_2$}-*closo*-2,1-$MoCB_{10}H_8$][15] or [4-(η^3-C_3H_5)-3,7,8-{$RuCl(PPh_3)_2$}-3,7,8-(μ-H)$_3$-4,1,6-*closo*-$NiC_2B_{10}H_9$],[7d] a fact that can be rationalized if one takes into account the steric demand and electronic differences of the exopolyhedral ruthenium fragments. In the present case it consists of the formally zwitterionic [$Ru(PPh_3)_2(SnB_{11}H_{11})$] moiety while the literature deals with the cationic $[RuCl(PPh_3)_2]^+$ fragment.

Conclusion

Stanna-*closo*-dodecaborate behaves as a two-faced, ambidentate ligand towards the ruthenium fragments $[Ru(PPh_3)_2]^{2+}$ and $[Ru(dppb)]^{2+}$. It is remarkable that the heteroborate can employ either η^1(Sn) coordination or η^3(B–H) coordination to bind to a ruthenium fragment and also has the ability to bridge two ruthenium fragments using both coordination modes at the same time. While the latter geometry imposes a rigid configuration, the tridentate B–H coordination alone displays fluxional behavior.

Experimental Section

General: All manipulations were carried out under dry argon in Schlenk glassware; solvents were dried and purified by standard methods and stored under argon. Elemental analyses were performed by the Institut für Anorganische Chemie Universität Tübingen using a Vario EL analyser. Chemicals were purchased commercially except $Na_2[SnB_{11}H_{11}]$,[23] $[Bu_3MeN]_2[SnB_{11}H_{11}]$,[19] $[RuCl_2(PPh_3)_3]$,[24] and $[RuCl_2(dppb)(PPh_3)]$,[25] which were prepared according to literature methods or modifications thereof.

X-ray data collection and refinement parameters:[26] X-ray data for compounds **2**, **3**, and **4** were collected on the diffractometers specified in Table 4 and were corrected for Lorentz and polarization effects and absorption by air. Numerical absorption correction based on crystal-shape optimization was applied for all data.[27] The programs used in this work are Stoe's X-Area,[28] including X-Red and X-Shape for data reduction and absorption correction,[29] and the WinGX suite of programs,[30] including SHELXS[31] and SHELXL,[32] for structure solution and refinement.

In the structure solution of **2** all hydrogen atoms were visible in the difference maps and were allowed to refine isotropically except those of the CH_2Cl_2 molecule, which were treated as riding atoms.

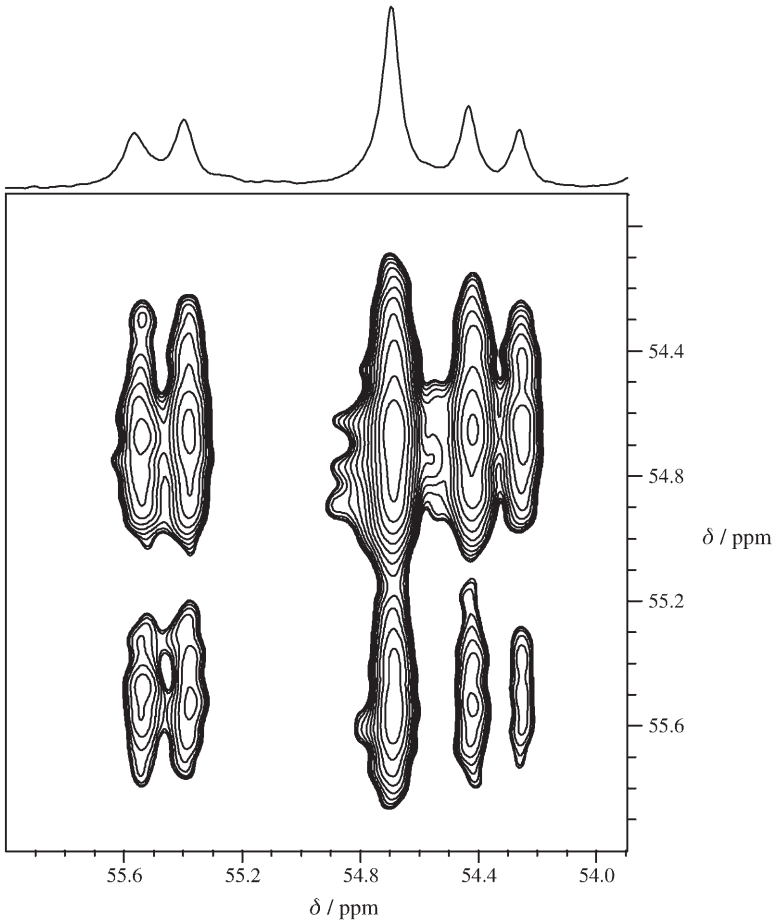

Figure 8. $^{31}P\{^{1}H\}$ EXSY NMR at room temperature of compound **5** in CD_2Cl_2.

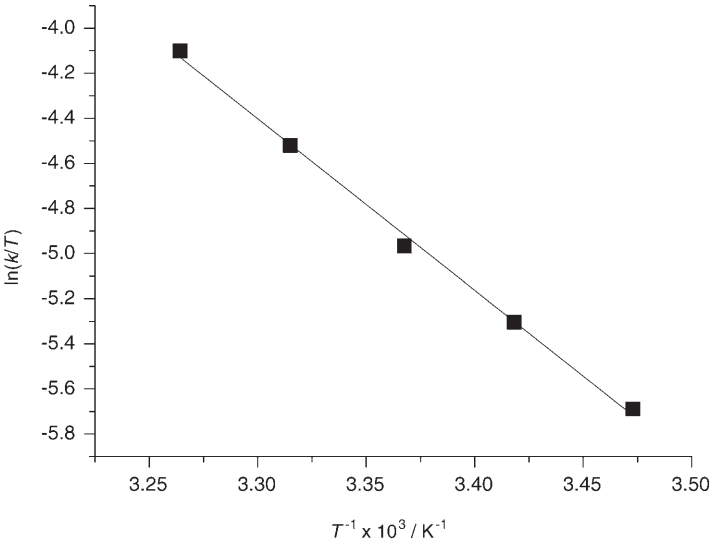

Figure 9. Eyring plot for compound **5**.

Table 3. Activation parameters for **5** from selective inversion experiments.

	$\Delta G^{\neq}_{298}$ [kJ mol^{-1}]	$\Delta H^{\neq}$ [kJ mol^{-1}]	$\Delta S^{\neq}$ [J mol^{-1} K^{-1}]
compound **5**	70.8 (±0.2)	62.7 (±1.8)	−27.1 (±6.2)

During the refinement of the structure of **3** all hydrogen atoms were located on difference maps except the phenyl hydrogen atom H233, which was calculated as riding. Because of disorder in the acetone solvent molecule present in the asymmetric unit, the acetone molecule was refined anisotropically without hydrogen atoms.

The disorder present in the structure of **4**, in which the B–H-coordinated $[SnB_{11}H_{11}]^{2-}$ is bonded to ruthenium in two different orientations, was refined by constraining the heteroborate icosahedron to a variable-metric rigid group using the AFIX 9 constraint. The two stannaborate moieties exhibit occupancies of 0.833(2) and 0.167(2) and the boron atoms of the minor stannaborate cage were refined isotropically. Another disorder over two sites was evident in one of the countercations' butyl chains and the carbon atoms involved were refined isotropically to occupancies of 0.59(2) and 0.41(2). DFIX, SAME, and DELU constraints were applied during the refinement of two other butyl groups. The B–H–Ru hydrogen atoms of the major $[SnB_{11}H_{11}]^{2-}$ cage were located on difference maps and H6 and H7 were freely refined, while H1 was positioned at the coordinates obtained and not refined. The other hydrogen atoms of the major species were included in the refinement cycles as riding atoms except the hydrogen bonded to B5, which was omitted. The hydrogen atoms of the minor stannaborate cluster were omitted also. All other hydrogen atoms of the ruthenium complex and the two countercations were kept at calculated positions.

NMR spectroscopy: NMR spectra were obtained from CD_2Cl_2 solutions using a Bruker DRX-250 NMR spectrometer equipped with a 5-mm ATM probe head and operating at 200.13 (^{1}H), 80.25 (^{11}B), 101.25 (^{31}P), and 93.25 MHz (^{119}Sn). Chemical shifts are reported in δ values relative to external TMS (^{1}H), $BF_3{\cdot}Et_2O$ (^{11}B), 85% aq. H_3PO_4 (^{31}P), or $SnMe_4$ (^{119}Sn) using the chemical shift of the solvent ^{2}H resonance frequency, 5.32 ppm.

Selective $^{31}P\{^{1}H\}$ inversion transfer experiments were acquired on a Bruker DRX-400 NMR spectrometer equipped with a 5-mm QNP probe head and using a (DANTE–τ–$\theta_{\text{non-selective}}$–acquire) pulse sequence. The DANTE sequence[33] consisted of 140 pulses of 0.175 μs duration spaced by 0.1 ms, corresponding to 24.5 μs for a flip angle of 180°, and was irradiated at the frequency of the A_2 system. Nonselective $^{31}P\{^{1}H\}$ inversion-recovery experiments were carried out on the same instrument in order to determine the spin-lattice relaxation times. For both experiments, 16 variable delays in the 0.1 ms–5 s range were applied and 32 scans acquired for each delay. The sample temperature was stabilized with a Bruker BDCT temperature controller and equilibrated for 15 min prior to acquisition. The actual temperature was determined by using the method of van Geet.[34] Exchange and spin-lattice relaxation rate constants were obtained from nonlinear least-squares fitting of the intensity data to expressions for two-site systems with equal populations in the slow-exchange regime,[35] using the ORIGIN program from OriginLab Corp. In a first step, spin-lattice relaxation rate constants were obtained from the inversion-recovery data and kept fixed in the second step, the analysis of the selective inversion-transfer experiments. Analysis of rate

Table 4. Crystal data and structure refinement parameters for **2**, **3**, and **4**.

	2	**3**	**4**
empirical formula	$C_{58}H_{82}B_{22}Cl_4P_4Ru_2Sn_2$	$C_{39}H_{47}B_{11}OP_2RuSn$	$C_{54}H_{110}B_{22}N_2P_2RuSn_2$
formula weight [g mol^{-1}]	1722.26	932.38	1425.65
diffractometer	STOE IPDS I	STOE IPDS II	STOE IPDS 2T
temperature [K]	220(2)	170(2)	173(2)
wavelength [Å]	0.71073	0.71073	0.71073
crystal system	monoclinic	monoclinic	monoclinic
space group	$P2_1/c$	$P2_1/n$	$P2_1/n$
a [Å]	12.778(2)	13.390(1)	11.942(1)
b [Å]	18.547(3)	16.830(2)	42.891(2)
c [Å]	18.889(3)	18.463(2)	14.468(1)
β [°]	125.696(16)	96.746(7)	103.971(4)
volume [Å^3]	3635.6(10)	4131.9(7)	7191.3(6)
Z	2	4	4
ρ_{calcd} [Mg m^{-3}]	1.573	1.499	1.317
μ [mm^{-1}]	1.360	1.080	0.976
F(000)	1712	1872	2928
crystal size [mm^3]	$0.22\times0.20\times0.16$	$0.2\times0.1\times0.1$	$0.22\times0.17\times0.16$
θ range for data collection [°]	2.25–26.02	1.64–27.32	2.91–23.59
index ranges	$-15\le h\le15$, $-22\le k\le22$, $-23\le l\le23$	$-17\le h\le16$, $-21\le k\le21$, $-23\le l\le22$	$-12\le h\le13$, $-48\le k\le48$, $-16\le l\le16$
reflections collected	43407	39668	27117
independent reflections	7111 [R(int) = 0.0568]	9147 [R(int) = 0.1092]	10361 [R(int) = 0.0424]
completeness to theta [%]	99.3	98.0	96.2
absorption correction	numerical	numerical	numerical
max. and min. transmission	0.8364 and 0.7696	0.8956 and 0.8182	0.9031 and 0.8489
refinement method	full-matrix least-squares on F^2	full-matrix least-squares on F^2	full-matrix least-squares on F^2
data/restraints/parameters	7111/0/571	9147/0/657	10361/16/734
goodness-of-fit on F^2	0.922	0.762	1.037
final R indices [$I>2\sigma$(I)]	$R1$ = 0.0292, $wR2$ = 0.0642	$R1$ = 0.0399, $wR2$ = 0.0554	$R1$ = 0.0644, $wR2$ = 0.1657
R indices (all data)	$R1$ = 0.0464, $wR2$ = 0.0686	$R1$ = 0.1065, $wR2$ = 0.0653	$R1$ = 0.0860, $wR2$ = 0.1794
largest diff. peak and hole [e Å^{-3}]	0.918 and −0.495	1.154 and −1.078	2.261 and −1.041

constant data was performed with ACTPAR,[36] a nonlinear least-squares program that considers errors in both dimensions.

2D $^{31}P\{^1H\}$ EXSY NMR spectra were recorded at room temperature using the Bruker pulse sequence noesyph, modified to provide ^1H broadband decoupling during detection in the phase-sensitive States-TPPI mode. A total of 16 scans per FID of 256 data points were collected for each of the 512 time increments. The recycle time was 5 s, over five times the measured T_1 values, the mixing time was 0.8 s.

NMR spectra of solid samples were obtained on a Bruker DSX-200 NMR spectrometer operating at 200.13 (^1H), 81.01 (^{31}P), and 74.60 MHz (^{119}Sn). The powdered samples were spinning about the magic angle at 10 kHz in 4-mm o.d. zirconia rotors. ^{31}P NMR spectra were obtained after variable-amplitude cross-polarization from protons and under high-power ^1H decoupling. ^{119}Sn NMR spectra were obtained after single-pulse excitation and under high-power ^1H decoupling. Chemical shifts are referenced with respect to external 85% aq. H_3PO_4 (^{31}P) or $SnMe_4$ (^{119}Sn) using the chemical shift of ammonium dihydrogen phosphate δ = 0.81 ppm, or $SnCy_4$ δ = −97.35 ppm, as secondary chemical shift reference.

$[Ru(dppb)(SnB_{11}H_{11})]_2$ (2): $[RuCl_2(dppb)(PPh_3)]$ (430.4 mg, 0.5 mmol) and $Na_2[SnB_{11}H_{11}]$ (147.3 mg, 0.5 mmol) were dissolved in THF (40 mL) and the resulting green solution was refluxed. After 1 h the solution turned orange-red and an orange precipitate had formed. Refluxing was continued for 60 h. The precipitate was filtered off, washed with water (3×20 mL), and dried under reduced pressure. Single crystals were obtained by slow evaporation from a CH_2Cl_2 solution (yield: 58.2 mg, 0.038 mmol, 15%). ^1H NMR (250 MHz, CD_2Cl_2): δ = 6.90–7.70 (m, 20H; $P(C_6H_5)_3$), 2.92 (br m; CH_2), 2.55 (br m; CH_2), 2.21 (br m; CH_2), 1.95 (br m; CH_2), −4.9 (br; Ru−H−B), −8.3 ppm (br; Ru−H−B); $^{11}B\{^1H\}$ NMR (128 MHz, CD_2Cl_2): δ = −10.8 (br), −15.0 (br), −20.7 (br), −31.7 ppm (Ru−H−B); $^{31}P\{^1H\}$ NMR (101 MHz, CD_2Cl_2): δ = 52.2 ppm (s, $^2J(^{117,119}Sn,P)$ = 275 Hz); elemental analysis calcd (%) for $C_{56}H_{78}B_{22}P_4Ru_2Sn_2$: C 43.32, H 5.06; found: C 42.56, H 4.95.

$[Ru(PPh_3)_2(SnB_{11}H_{11})]_2$ (3): $[RuCl_2(PPh_3)_3]$ (479.4 mg, 0.5 mmol) and $Na_2[SnB_{11}H_{11}]$ (147.3 mg, 0.5 mmol) were dissolved in THF (40 mL) and the resulting dark brown solution was refluxed. After 1 h the solution had turned deep red and an orange precipitate had formed. Refluxing was continued for 60 h to maximize the amount of precipitate. The precipitate was filtered off, washed with water (3×20 mL), and dried under reduced pressure. Single crystals were obtained by slow evaporation from an acetone solution (yield: 93.2 mg, 0.053 mmol, 21.2%). Elemental analysis calcd (%) for $C_{72}H_{82}B_{22}P_4Ru_2Sn_2$: C 49.45, H 4.73; found: C 48.81, H 4.97.

$[Bu_3MeN]_2[Ru(dppb)(2,7,8\text{-}(\mu\text{-}H)_3\text{-}exo\text{-}SnB_{11}H_{11})(SnB_{11}H_{11})]$ (4): A solution of $[Bu_3MeN]_2[SnB_{11}H_{11}]$ (649.5 mg, 1 mmol) in CH_2Cl_2 (10 mL) was added by syringe to a dark green solution of $[RuCl_2(dppb)(PPh_3)]$ (430.4 mg, 0.5 mmol) in CH_2Cl_2 (10 mL) to give a red-brown solution, which was stirred for an additional 2 h at room temperature. The CH_2Cl_2 solution was then extracted with water (3×20 mL) to remove $[Bu_3MeN]Cl$. Removal of the CH_2Cl_2 under reduced pressure yielded a red-brown solid which was washed with Et_2O (5×20 mL). The residue was recrystallized from CH_2Cl_2/Et_2O to give dark orange prisms (yield: 0.57 g, 0.4 mmol, 80%). ^1H NMR (without $[Bu_3MeN]^+$) (250 MHz, CD_2Cl_2): δ = 7.15–7.95 (m, 20H; $P(C_6H_5)_2$), 3.2–3.6 (br m; CH_2), 2.7–3.1 (br m; CH_2), 1.8–2.2 (br m; CH_2), −6.4 (br; Ru−H−B), −7.5 ppm (br; Ru−H−B); $^{11}B\{^1H\}$ (128 MHz, CD_2Cl_2): δ = −1.6 (br), −8.0 (br), −15.2 (br), −19.9 (br), −22.4 ppm (Ru−H−B); $^{31}P\{^1H\}$ NMR (101 MHz, CD_2Cl_2): δ = 51.6 (d, ^2J(P,P) = 35.4 Hz, $^2J(^{117,119}Sn,P)$ = 273 Hz), 51.5 (s, $^2J(^{117,119}Sn,P)$ = 267 Hz), 51.0 ppm (d, ^2J(P,P) = 35.4 Hz, $^2J(^{117,119}Sn,P)$ = 273 Hz); ^{119}Sn NMR (149 MHz, CD_2Cl_2): δ = −366, −374, −630, −638 ppm; elemental analysis calcd (%) for $C_{54}H_{110}B_{22}N_2P_2RuSn_2$: C 45.49, H 7.78, N 1.96; found: C 45.37, H 7.93. N 1.96.

$[Bu_3MeN]_2[Ru(PPh_3)_2(2,7,8\text{-}(\mu\text{-}H)_3\text{-}exo\text{-}SnB_{11}H_{11})(SnB_{11}H_{11})]$ (5): A solution of $[Bu_3MeN]_2[SnB_{11}H_{11}]$ (259.8 mg, 0.4 mmol) in CH_2Cl_2 (10 mL) was added by syringe to a solution of $RuCl_2(PPh_3)_3$ (191.8 mg, 0.2 mmol) in CH_2Cl_2 (10 mL). The mixture was stirred for 24 h to give an orange-red solution, which was then extracted with water (3×20 mL) to remove $[Bu_3MeN]Cl$. Removal of CH_2Cl_2 under reduced pressure yielded an orange-red solid, which was washed with Et_2O (5×20 mL) and dried under reduced pressure overnight (yield: 234.7 mg, 0.15 mmol, 77%). ^1H NMR (without $[Bu_3MeN]^+$) (250 MHz, CD_2Cl_2): δ = 6.95–7.60 (m, 20H; $P(C_6H_5)_3$), −7.0 to −7.6 ppm (br; Ru−H−B); $^{11}B\{^1H\}$ (128 MHz, CD_2Cl_2): δ = −2.1 (br), −8.9 (br), −15.3 (br), −20.9 ppm (br); $^{31}P\{^1H\}$ NMR (101 MHz, CD_2Cl_2): δ = 55.4 (d, ^2J(P,P) = 27.7 Hz, $^2J(^{117,119}Sn,P)$ = 260 Hz), 54.6 (s, $^2J(^{117,119}Sn,P)$ = 263 Hz), 54.2 ppm (d, ^2J(P,P) = 27.7 Hz, $^2J(^{117,119}Sn,P)$ = 260 Hz); ^{119}Sn NMR (149 MHz, CD_2Cl_2): δ = −398, −628, −640 ppm; elemental analysis calcd (%) for $C_{72}H_{82}B_{22}P_4Ru_2Sn_2$: C 49.45, H 4.73; found: C 48.81, H 4.97.

Acknowledgements

Financial support from the Deutsche Forschungsgemeinschaft is gratefully acknowledged.

[1] a) L. Barton, D. K. Srivastava in *Comprehensive Organometallic Chemistry II, Vol. 2*, (Eds.: E. W. Abel, F. G. A. Stone, G. Wilkinson), Pergamon, Oxford, **1995**, pp. 275–372; b) R. N. Grimes in *Comprehensive Organometallic Chemistry II, Vol. 2*, (Eds.: E. W. Abel, F. G. A. Stone, G. Wilkinson), Pergamon, Oxford, **1995**, pp. 373–430.

[2] For example: a) S. Du, J. A. Kautz, T. D. McGrath, F. G. A. Stone, *Angew. Chem.* **2003**, *115*, 5906–5908; *Angew. Chem. Int. Ed.* **2003**, *42*, 5728–5730; b) S. A. Batten, J. C. Jeffrey, P. L. Jones, D. F. Mullica, M. D. Rudd, E. L. Sappenfield, F. G. A. Stone, A. Wolf, *Inorg. Chem.* **1997**, *36*, 2570–2577; c) S. Du, J. C. Jeffery, J. A. Kautz, X. L. Lu, T. D. McGrath, T. A. Miller, T. Riis-Johannessen, F. G. A. Stone, *Inorg. Chem.* **2005**, *44*, 2815–2825.

[3] S. Bresadola, P. Rigo, A. Turco, *J. Chem. Soc. Chem. Commun.* **1968**, 1205–1206.

[4] S. V. Ivanov, J. J. Rockwell, O. G. Polyakov, C. M. Gaudinski, P. Anderson, K. A. Solntsev, S. H. Strauss, *J. Am. Chem. Soc.* **1998**, *120*, 4224–4225.

[5] T. E. Paxson, M. F. Hawthorne, L. D. Brown, W. N. Lipscomb, *Inorg. Chem.* **1974**, *13*, 2772–2774.

[6] M. Elrington, N. N. Greenwood, J. D. Kennedy, M. J. Thornton-Pett, Mark, *J. Chem. Soc. Dalton Trans.* **1987**, 451–456.

[7] a) D. D. Ellis, P. A. Jelliss, F. G. A. Stone, *Organometallics* **1999**, *18*, 4982–4994; b) I. V. Pisareva, V. E. Konoplev, P. V. Petrovskii, E. V. Vorontsov, F. M. Dolgushin, A. I. Yanovsky, I. T. Chizhevsky, *Inorg. Chem.* **2004**, *43*, 6228–6237; c) B. E. Hodson, T. D. McGrath, F. G. A. Stone, *Organometallics* **2005**, *24*, 1638–1646; d) B. E. Hodson, T. D. McGrath, F. G. A. Stone, *Dalton Trans.* **2004**, 2570–2577.

[8] a) F. Teixidor, J. A. Ayllón, C. Viñas, R. Kivekäs, R. Sillanpäa, J. Casabó, *Organometallics* **1994**, *13*, 2751–2760; b) C. Viñas, R. Nuñez, M. A. Flores, F. Teixidor, R. Kivekäs, R. Sillanpäa, *Organometallics* **1995**, *14*, 3952–3957; c) C. Viñas, R. Nuñez, F. Teixidor, R. Kivekäs, R. Sillanpäa, *Organometallics* **1996**, *15*, 3850–3858; d) F. Teixidor, M. A. Flores, C. Viñas, R. Kivekäs, R. Sillanpäa, *Organometallics* **1998**, *17*, 4675–4679.

[9] L. Wesemann, T. Marx, U. Englert, M. Ruck, *Eur. J. Inorg. Chem.* **1999**, 1563–1566.

[10] T. Marx, B. Mosel, I. Pantenburg, S. Hagen, H. Schulze, L. Wesemann, *Chem. Eur. J.* **2003**, *9*, 4472–4478.

[11] T. Marx, L. Wesemann, S. Dehnen, I. Pantenburg, *Chem. Eur. J.* **2001**, *7*, 3025–3032.

[12] S. Hagen, I. Pantenburg, F. Weigend, C. Wickleder, L. Wesemann, *Angew. Chem.* **2003**, *115*, 1539–1543; *Angew. Chem. Int. Ed.* **2003**, *42*, 1501–1505.

[13] S. Hagen, L. Wesemann, I. Pantenburg, *Chem. Commun.* **2005**, 1013–1015.

[14] T. Marx, L. Wesemann, *J. Organomet. Chem.* **2000**, *614–615*, 137–143.

[15] D. D. Ellis, A. Franken, P. A. Jelliss, J. A. Kautz, F. G. A. Stone, P. Y. Yu, *J. Chem. Soc. Dalton Trans.* **2000**, 2509–2520.

[16] M. Holt, W. Wilson, J. Nelson, *Chem. Rev.* **1989**, *89*, 11–49.

[17] S. Hermanek, *Chem. Rev.* **1992**, *92*, 325–362.

[18] R. D. Adams, D. A. Katahira, *Organometallics* **1982**, *1*, 53–59.

[19] R. W. Chapman, J. G. Kester, K. Folting, W. E. Streib, L. J. Todd, *Inorg. Chem.* **1992**, *31*, 979–983.

[20] L. Carlton, *Inorg. Chem.* **2000**, *39*, 4510–4519.

[21] C. T. Hunt, A. L. Balch, *Inorg. Chem.* **1982**, *21*, 1641–1644.

[22] O. P. Charkin, N. M. Klimenko, D. Moran, A. M. Mebel, D. O. Charkin, P. V. R. Schleyer, *J. Phys. Chem. A* **2002**, *106*, 11594–11602.

[23] T. Marx, B. Ronig, H. Schulze, I. Pantenburg, L. Wesemann, *J. Organomet. Chem.* **2002**, *664*, 116–122.

[24] P. S. Hallman, T. A. Stephenson, G. Wilkinson, *Inorg. Synth.* **1970**, *12*, 237.

[25] C. W. Jung, P. E. Garrou, P. R. Hoffman, K. G. Caulton, *Inorg. Chem.* **1984**, *23*, 126–129.

[26] CCDC-276023 (**2**), CCDC-276024 (**3**), and CCDC-276025 (**4**) contain the supplementary crystallographic data for this paper. These data can be obtained free of charge from The Cambridge Crystallographic Data Centre via www.ccdc.cam.ac.uk/data_request/cif.

[27] X-Shape 2.05, Crystal Optimisation for Numerical Absorption Correction, STOE & Cie GmbH, Darmstadt, **1999**.

[28] X-AREA 1.26, Stoe & Cie GmbH, Darmstadt, **2004**.

[29] X-RED 1.26, Stoe Data Reduction Program, Stoe & Cie GmbH Darmstadt, **2004**.

[30] L. J. Farrugia, *J. Appl. Crystallogr.* **1999**, *32*, 837–838.

[31] G. M. Sheldrick, SHELXS-97, Program for the Solution of Crystal Structures, Göttingen, **1997**.

[32] G. M. Sheldrick, SHELXL-97, Program for Crystal Structure Refinement, Göttingen, **1997**.

[33] G. A. Morris, R. Freeman, *J. Magn. Reson.* **1978**, *29*, 433–462.

[34] a) A. L. van Geet, *Anal. Chem.* **1970**, *42*, 679; b) A. L. van Geet, *Anal. Chem.* **1968**, *40*, 2227–2229.

[35] A. D. Bain, J. A. Cramer, *J. Phys. Chem.* **1993**, *97*, 2884–2887.

[36] G. Binsch, H. Kessler, *Angew. Chem.* **1980**, *92*, 445–463; *Angew. Chem. Int. Ed. Engl.* **1980**, *19*, 411–429.

Received: July 1, 2005
Published online: October 26, 2005

